15th Triennial World Congress, Barcelona, Spain

DESIGN AND CONTROL OF A THERMAL STABILIZING SYSTEM FOR AN OPTOMECHANICAL UNCOOLED INFRARED IMAGING CAMERA

Jongeun Choi * **Joji Yamaguchi** [1] **Simon Morales** [2]
Roberto Horowitz * **Yang Zhao** * **Arun Majumdar** *
Paul Norton **

* *Department of Mechanical Engineering*
University of California, Berkeley, CA 94720-1740, USA
** *IR Vision, Santa Barbara, CA 93105, USA*

Abstract: In this paper, the design and control of a thermal stabilizing system for an Optomechanical Uncooled Infrared Imaging camera is presented, which uses an array of MEMS bimaterial cantilever beams to sense an infrared image source. A one-dimensional lumped parameter model of the thermal stabilization system was derived and experimentally validated. A model-based discrete time Linear Quadratic Gaussian Regulator(LQGR) control scheme, with a stochastic ambient noise model, was implemented. The control system incorporates a reference model, which generates desired reference temperature trajectory, and integral action to respectively diminish overshoots and achieve zero steady state error in closed loop. Simulation results show that the designed LQGR controller is able to enhance ambient temperature low frequency disturbance attenuation by more than 50dB. The control system is able to regulate the focal-plane array (FPA) temperature with a standard deviation of about 100μK, in spite of the fact that the temperature measurement noise has a standard deviation of $1m$K.

Keywords: MEMS IR sensors, Infrared image detectors, temperature control, LQG control, stochastic modeling,

1. INTRODUCTION

In many engineering applications involving temperature sensitivity issues, it is required that the temperature be regulated to within some operating range. Temperature stabilization systems have been discussed in many publications. Temperature regulators that utilize Peltier junction heat pumps and conventional PID controllers are commonly used nowadays (Sloman *et al.*, 1996).

The temperature control system design presented in this paper is part of a novel Optomechanical Uncooled Infrared Imaging system, which utilizes an array of MEMS bimaterial cantilever beams, and it is currently under development by the authors of this paper, (Zhao *et al.*, 2001*a*), (Zhao *et al.*, 2001*b*). Infrared (IR) vision is an indispensable technology for night vision, surveillance and navigation through obscure environments. Our uncooled IR imaging system consists of an absorption pad for IR radiation and a focal-plane array (FPA) of about 300×300 pixels, with each pixel containing a bimaterial cantilever beam built based on the MEMS technology, and shown in Fig. 1, (Zhao *et al.*, 2001*a*). A low-power visible laser

[1] Visiting scholar from Telecommunications Energy Labs. NTT, Atsugi-shi, Kanagawa 243-0198 Japan.
[2] Visiting scholar from IMME/EIE-FI, University Central of Venezuela, PO Box 50361, Caracas 1050-A, Venezuela.

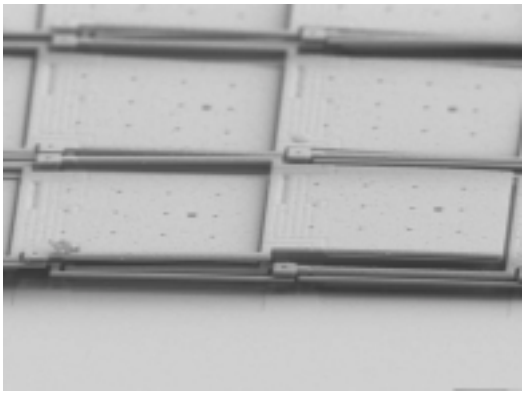

Fig. 1. FPA built on MEMS technology.

is used to measure cantilever deflections for the localized interferometry to project it onto a visible charge-coupled device (CCD). A first prototype of such an infrared system, which did not utilize a thermal control system such as the one presented in this paper, was described in (Perazzo *et al.*, 1999). The new design has MEMS cantilevers that have a much larger sensitivity than those in the design presented in (Perazzo *et al.*, 1999), requires that the FPA temperature be regulated to within a standard deviation of 100μK. This yields a Noise Equivalent Temperature Difference (NETD) standard deviation of 1.67mK (Zhao *et al.*, 2001*b*). The NETD of an IR imaging system represents the resolution of the target temperature, that can be measured by the device. This paper describe the design of a thermal stabilizing system for the IR imaging system. The design was carried out in two stages. In the first stage a passive thermal shield design was invented to maximize the attenuation of ambient temperature fluctuation while still maintaining a high sensitivity to the IR source. The second stage of the design involved feedback control. After obtaining stochastic models of the ambient temperature noise disturbances and sensor noise, a Kalman filter observer was designed to estimate the FPA temperature and a Linear Quadratic Gaussian Regulator was implemented to regulate the FPA temperature. The control system was designed in order to enhance low frequency ambient temperature disturbance attenuation without significantly degrading the device's sensitivity to the target IR temperature.

2. DESIGN AND MODELING

A SEM photograph of the fabricated FPA is shown in Fig. 1. A schematic depiction of the camera is shown in Fig. 2. The bimaterial cantilever deflection, as its temperature rises due to absorption of the incident infrared radiation, is proportional to the change in temperature of the beam and also to the difference between the thermal expansion coefficients of the two cantilever

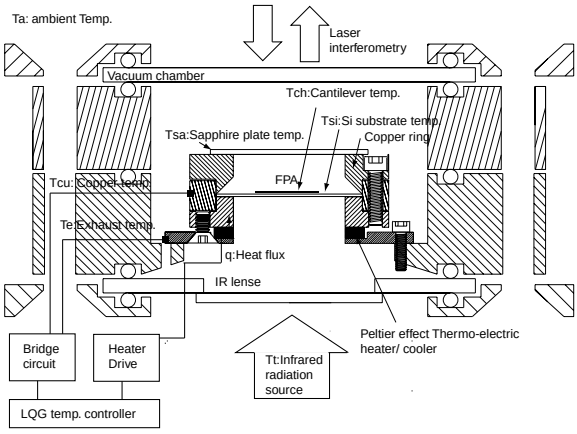

Fig. 2. A schematic setup of the IR camera and its temperature control system. The CCD and optical readout system is outside of the vacuum chamber.

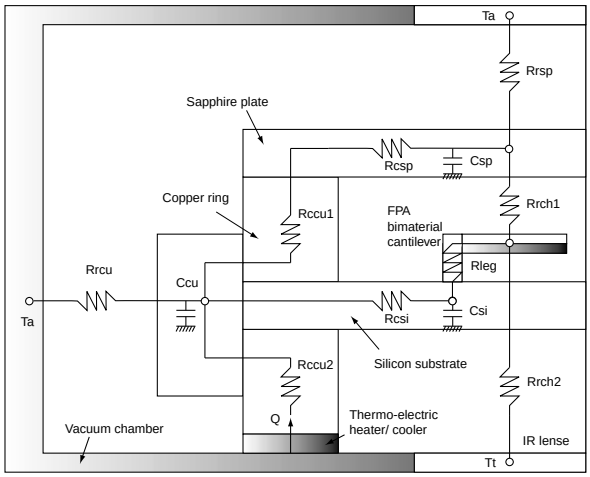

Fig. 3. A schematic diagram of lumped parameter modeling

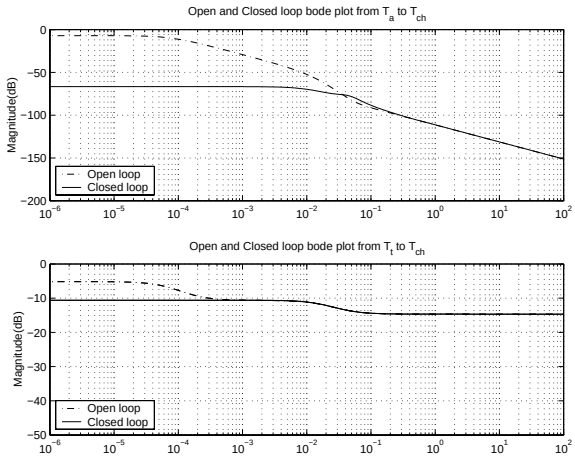

Fig. 4. Open loop and closed loop Bode plot for (1) T_a to T_{ch} and (2) T_t to T_{ch}. The systems are non-minimum phase.

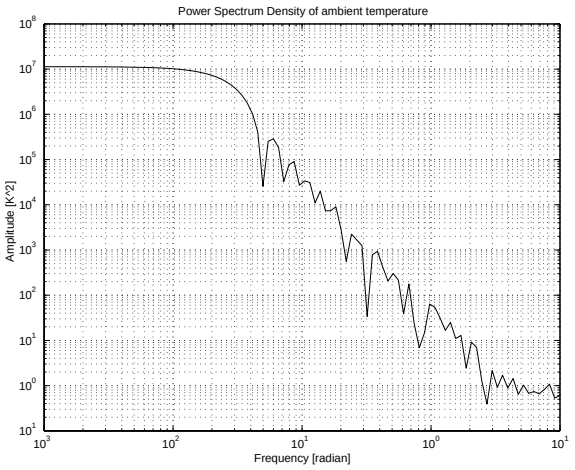

Fig. 5. Power spectrum density of ambient temperature.

materials. An optical system using visible light simultaneously measures the deflections of all the cantilevers of the FPA, and collectively projects a visible image of the spatially-varying IR radiation onto a visible CCD or CMOS array. As shown in Fig. 2, the FPA is surrounded by a heat shield, which consists of a copper cylinder and a thermally conductive sapphire plate. This shield isolates the FPA from fluctuations in the ambient temperature T_a. The sapphire plate is transparent to laser light, allowing the laser to be used as an interferometry measurement system to obtain an image from the FPA. A thermo-electric peltier junction heater/cooler comprises the thermal actuator, which is capable of adding heat to or removing heat from the system. A thermistor on the side of the copper ring senses its temperature T_{cu}. Another thermistor is attached to the vacuum chamber to measure the deterministic initial ambient temperature. The thermal shield has a low thermal resistance for the copper cylinder (R_{ccu1}), as shown Fig. 3 and so does the sapphire plate. However the thermal resistance between the FPA and the copper cylinder (R_{csi}) is chosen to be relatively high, in order to isolate the FPA from the regulated thermal shield. As a consequence, the thermal system provides a large amount of attenuation in open loop, ($-50 \sim -100$dB) in the range of ($0.002 \sim 10$Hz) from the disturbance T_a to FPA temperature T_{ch}, as shown in Fig. 4. An one-dimensional lumped parameter model was used to model the thermal system taking into account of thermal capacitance and thermal resistance of the copper block and sapphire and silicon plates in Fig. 3. Fig. 5 shows the power spectrum density of the measured ambient temperature in the lab where the IR imaging system is located. Based on this data, a model for the ambient temperature fluctuations was derived which consists of a critically damped second order linear dynamic system with a cut-off frequency of 2.5×10^{-2} $[rad]$, which is excited by zero mean

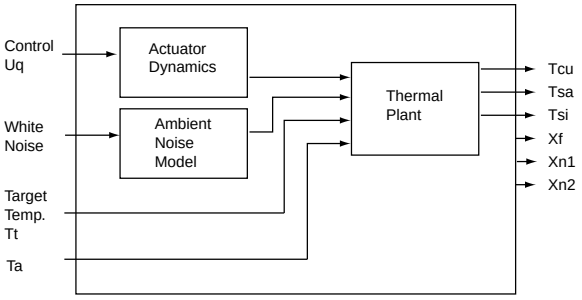

Fig. 6. Augmented system with a linearized thermal plant, an actuator model and an stochastic noise model.

white noise $w(t)$ $E(w(i)w(j)^T) = W\delta_{ij}$, where $W = 1600$ [K^2] (obtained from the measurement in Fig. 5) and δ_{ij} is the Kronecker delta. A high sensitivity thermistor and analog bridge circuit were used to measure the copper ring temperature with a 1mK measurement noise standard deviation.

3. CONTROL LAW

3.1 *The Kalman filter for the linearized plant*

The closed loop system was designed based on a discrete time linearized thermal plant which included the third order lumped parameter thermal model depicted in Fig. 3, the identified ambient temperature stochastic noise model and an empirically found actuator dynamics. An augmented system for the observer and the controller was constructed as shown in Fig. 6. The augmented system consists of the plant state $x_p = [T_{cu} \quad T_{sa} \quad T_{si}]^T$, where T_{cu} is the copper ring temperature, T_{sa} is the sapphire plate temperature and T_{si} is the silicon substrate temperature, the actuator state x_f and the noise model state $x_N = [x_{n1} \quad x_{n2}]^T$. The state x_N is not controllable from the control input $u_{q(t)}$ but is stable and it is only of a stochastic nature.

$$\begin{pmatrix} x_{p(t+1)} \\ x_{f(t+1)} \\ x_{N(t+1)} \end{pmatrix} = A_a \begin{pmatrix} x_{p(t)} \\ x_{f(t)} \\ x_{N(t)} \end{pmatrix} + B_a \begin{pmatrix} u_q \\ T_a \\ T_t \end{pmatrix} + G_a w(t)$$

i.e.,

$$\begin{aligned} X_{a(t+1)} &= A_{a(6\times6)} X_{a(t)} + B_{a(6\times3)} u_{a(t)} + G_a w(t) \\ y_{a(t)} &= C_a X_{a(t)} + v(t), \end{aligned} \tag{1}$$

where $w(t)$ and $v(t)$ are white noises, which have the following properties

$$\begin{aligned} E(w(t)) = 0, \quad E(w(i)w(j)^T) = W\delta_{ij} \\ E(v(t)) = 0, \quad E(v(i)v(j)^T) = V\delta_{ij}. \end{aligned}$$

In addition, the deterministic mean values of the ambient and target temperatures, respectively T_a and T_t, are also considered as inputs to the

system given by Eq. (1) and depicted in Fig. 6. The output of this system is the copper cylinder temperature T_{cu} and only T_{cu} is penalized by the controller. Therefore, the corresponding B_a and C_a are

$$B_a = [B_{a1(6\times1)} \quad B_{a2(6\times1)} \quad B_{a3(6\times1)}]$$
$$C_a = [1 \quad 0 \quad 0 \quad 0 \quad 0 \quad 0].$$

Given the detectable pair (A_a, C_a) and the stabilizable (A_a, B_a), there exists a steady state Kalman filter gain, which is given by $M_s = \Sigma_s C^T (C\Sigma_s C^T + V)^{-1}$, where Σ_s is the solution of the following algebraic Riccati equation

$$\begin{aligned}\Sigma_s = A_a \Sigma_s A_a^T + G_a W G_a^T \\ -A_a \Sigma_s C^T (C\Sigma_s C^T + V)^{-1} C \Sigma_s A_a^T.\end{aligned} \tag{2}$$

Using the Kalman filter gain M_s from Eq. (2) and the system parameters in Eq. (1), an optimal state estimator can be constructed as follows

$$\begin{aligned}\hat{X}_{a(t+1|t+1)} = (I - M_s C_a) A_a \hat{X}_{a(t|t)} \\ +(I - M_s C_a) B_a u_t + M_s y_{t+1}.\end{aligned} \tag{3}$$

3.2 *Integral action and reference model for the desired trajectory*

An integral action control was implemented to compensate for the detrimental effects of constant disturbances (Bitmead *et al.*, 1990). Define the tracking error as $e_t = y_a - y_r$, where $y_a = T_{cu}$ is the copper ring temperature and $y_r = T_{cur}$ is the reference temperature trajectory. The incremental tracking error integral is given by

$$I_{t+1} = I_t + e_t = I_t + C_a X_a - y_r. \tag{4}$$

A second order linear dynamic system with an unit static gain was chosen for the reference model.

$$\begin{aligned}x_{r(t+1)} = A_{r(2\times2)} x_{r(t)} + B_{r(2\times1)} u_{r(t)} \\ y_{r(t)} = C_{r(1\times2)} x_{r(t)}\end{aligned} \tag{5}$$

Utilizing Eq. (5) and Eq. (4) with the plant model Eq. (1) the linear quadratic tracking problem can be reformulated into a standard linear quadratic regulation of the following composite system with an extended state.

$$x_t^{track} = \begin{pmatrix} X_{a(t)} \\ I_t \\ x_{r(t)} \end{pmatrix}$$

The state equation for x_t^{track} is then obtained by combining the state equations of $X_{a(t)}$, I_t and $x_{r(t)}$. $u_{r(t)}$ is a constant set-point.

$$\begin{aligned}x_{t+1}^{track} = \begin{bmatrix} A_{a(6\times6)} & 0_{6\times1} & 0_{6\times2} \\ C_a & 1 & -C_{r(1\times2)} \\ 0_{2\times6} & 0_{2\times1} & A_{r(2\times2)} \end{bmatrix} x_t^{track} \\ + \begin{bmatrix} B_{a1(6\times1)} & 0_{7\times1} \\ 0_{3\times1} & B_{r(2\times1)} \end{bmatrix} \begin{pmatrix} u_{q(t)} \\ u_{r(t)} \end{pmatrix}\end{aligned} \tag{6}$$

y_t^{track} is given by

$$\begin{aligned}y_t^{track} = (y_{a(t)} - y_{r(t)}) + g_e I_t \\ = C^{track} x_t^{track} = [C_a \quad g_e \quad -Cr] x_t^{track},\end{aligned} \tag{7}$$

where g_e is the weighting factor between the tracking error and the incremental tracking error. Multiplying the each side of Eq. (6) by the difference operator $(1 - q^{-1})$ and considering $u_{r(t)}$ to be a constant desired set-point leads to

$$\begin{pmatrix} x_{d(t)} \\ e_t \\ x_{rd(t)} \end{pmatrix} = A^{track} \begin{pmatrix} x_{d(t-1)} \\ e_{t-1} \\ x_{rd(t-1)} \end{pmatrix} + \begin{bmatrix} B_{a1(6\times1)} \\ 0_{3\times1} \end{bmatrix} ((1 - q^{-1}) u_q = v_{t-1})$$

i.e.,

$$\begin{aligned}x_{d(t)}^{track} = A^{track} x_{d(t-1)}^{track} + B^{track} v_{t-1} \\ y_{d(t-1)}^{track} = C_a x_{d(t-1)} - C_r x_{rd(t-1)} + g_e e_{t-1},\end{aligned} \tag{8}$$

where $x_{d(t-1)} = (1 - q^{-1}) X_{a(t)}$ and $x_{rd(t-1)} = (1 - q^{-1}) x_{r(t)}$, while the tracking criteria performance index can be written as

$$J = \sum_{t_0}^{\infty} \{(x_{d(t)}^{track})^T Q^{track} (x_{d(t)}^{track}) + \nu_t^T R^{track} \nu_t\}. \tag{9}$$

where $x_{d(t)}^{track} = (1 - q^{-1}) x_{t+1}^{track}$, $\nu_t = (1 - q^{-1}) u_{q(t+1)}$, $Q^{track} = C^{trackT} C^{track}$ and $R^{track} > 0$ is a weighting factor for the incremental control input ν_t. Therefore, the optimal control having penalty on the error and the incremental error is given by

$$\begin{aligned}u_{q(t)} = -K^{track} x_t^{track} \\ = -K_a x_{a(t))} - K_r x_{r(t)} - K_e \sum_{t_0}^{t-1} e_t,\end{aligned} \tag{10}$$

where the optimal control gain matrix is given by

$$\begin{aligned}K^{track} = [K_{a(1\times6)} \quad K_{e(1\times1)} \quad K_{r(1\times2)}] \\ = (R^{track} + B^{track} P B^{track})^{-1} B^{trackT} P A^{track}\end{aligned}$$

and P is the solution of the following algebraic Riccati equation

$$\begin{aligned}A^{trackT} P A^{track} - P - A^{trackT} P B^{track} K^{track} \\ +Q^{track} = 0.\end{aligned} \tag{11}$$

A block diagram of the overall LQG control system with integral action and desired temperature trajectory tracking is shown in Fig. 7. This controller guarantees the rejection of a constant disturbance and tracking of a desired temperature.

4. RESULTS AND DISCUSSION

The temperature control system described in Fig. 2 was built and assembled by the authors. This

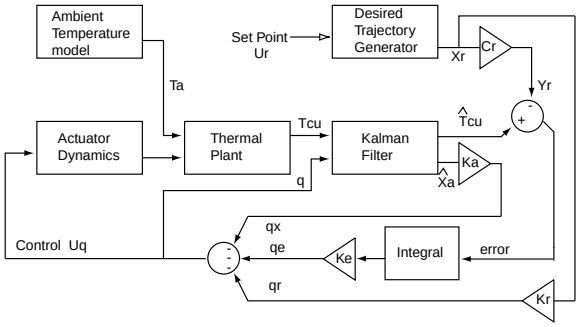

Fig. 7. LQG with desired trajectory control scheme

included a vacuum chamber ($1m$ Torr) and the temperature shield consisting of the copper ring and the sapphire plate. An analog amplifer to drive the thermo-electric heater/cooler and a low-noise bridge circuit for the thermistors were also costume designed and built. An optical readout system to produce the images from infrared source was also constructed. The control algorithm with a sampling time of 0.1[sec] was written in the 'C ' programming language on a personal computer using a Data Translation DT322 16 bits analog-to-digital and digital-to-analog converters. The thermistor on the bottom of the heat sink chamber was used to measure the ambient temperature T_a. Its mean value was experimentally determined and it was used as the value of the deterministic disturbance temperature. The real time measurement of T_a was also used to linearized the dynamics of the thermo-electric heater/cooler using an algorithm described in (Sloman *et al.*, 1996). Several typical experimental results are presented and described in this section. A comprehensive simulation study allowed us to select the initial values for the control parameters g_e in Eq. (7), R^{track} in Eq. (9) and the DC gain and the time constant of the thermo-electic heater/cooler model. Model identification and validation was based on matching transient responses. Appropriate model parameters were chosen so that the experimental and simulated results closely resembled each other, as shown in Fig. 8 and in Fig. 9. Parameters of the thermo-electric heater/cooler model change easily depending on operating conditions such as the chamber vacuum level, the quantity of thermal conductive paste that was used between the heater/cooler and the chamber floor and the operating temperature of the FPA. The heater/cooler model parameters were subsequently retuned to match the experimentally determined state estimation covariances to their corresponding simulation values, as shown in Table 1. However, transient responses in the experiment exhibited oscillatory modes, as the control penalty gain R^{track} was decreased, which were not observed in the simulation results. This is attributed to unmodeled dynamics between the copper ring and

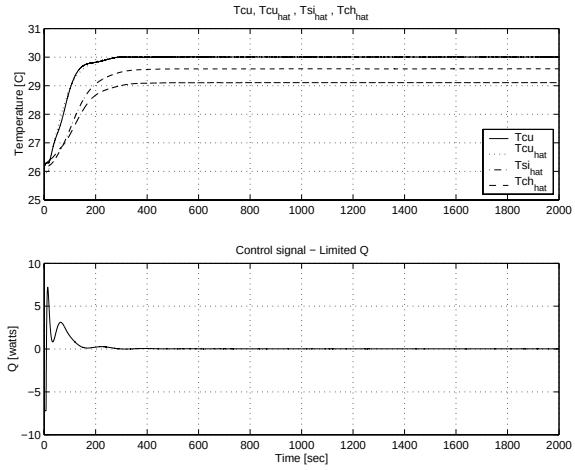

Fig. 8. Experimental results with $g_e = 1, R^{track} = 10$. $T_{cu}^{measured}$, $\hat{T}_{cu}$, $\hat{T}_{si}$ and $\hat{T}_{ch}$.

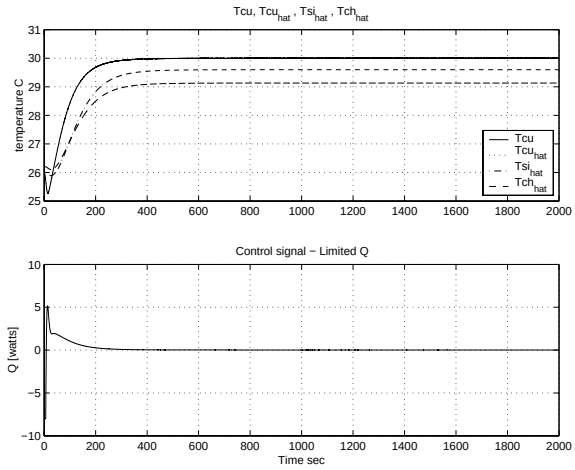

Fig. 9. Simulation Results with $g_e = 1, R^{track} = 10$. $T_{cu}^{measured}$, $\hat{T}_{cu}$, $\hat{T}_{si}$ and $\hat{T}_{ch}$.

chip temperatures. Table 1 shows that simulation and the experimental results are in close agreement. With a copper ring temperature measurement noise that has a 1mK standard deviation, the FPA T_{ch} temperature could be regulated to within a standard deviation of about 100μK. As shown in Table 1, the standard deviation of the FPA T_{ch} temperature is about twice as that of T_{cu}, due to the relatively large fluctuation in the sapphire plate temperature which had a standard deviation of $8.92m$K in the simulation results. Fig. 10 shows a close up of the steady state response for the measured copper temperature T_{cu}, the estimated copper temperature $\hat{T}_{cu}$, the estimated silicon temperature $\hat{T}_{si}$, as well as the estimated FPA temperature $\hat{T}_{ch}$. The Kalman filter output $\hat{T}_{cu}$ estimates well the measured temperature T_{cu}.

5. CONCLUSION

This paper presented the design and control of a thermal stabilizing system for an Optomechanical Uncooled Infrared Imaging camera. Experiments

Table 1. Steady state simulated and experimental results of the LQG control with penalty on the copper temperature T_{cu} with $g_e = 1, R^{track} = 0.1$.

Std Deviation	Unit	Simulation	Experiment
$\sigma_{T_{cu}}^{measured}$	mK	1.013	1.131
$\sigma_{\hat{T}_{cu}}$	μK	46.43	61.52
$\sigma_{\hat{T}_{si}}$	μK	69.23	73.77
$\sigma_{\hat{T}_{ch}}$	μK	120.0	117.3

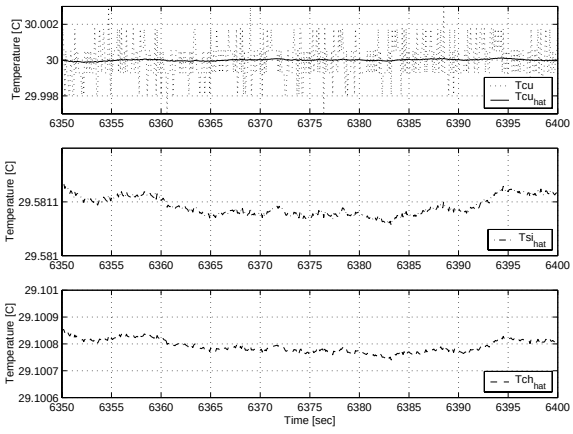

Fig. 10. Close up of the steady state experimental results with $g_e = 1, R^{track} = 0.1$. (1) $T_{cu}^{measured}$ and $\hat{T}_{cu}$ (2) $\hat{T}_{si}$ (3) $\hat{T}_{ch}$.

showed successful results for the prototype camera with the optical readout system. The thermal shield system provides a large amount of attenuation in open loop from disturbances in the ambient temperature T_a to FPA temperature T_{ch}. A carefully designed ambient temperature disturbance model was used to represent ambient temperature fluctuations, and this model was subsequently used in a model based discrete Linear Quadratic Gaussian Regulator(LQGR) control scheme. The LQGR controller was able to achieve an additional low frequency attenuation of more than 50dB of disturbance rejection from the ambient temperature T_a to the FPA temperature T_{ch}. The disturbance attenuation was achieved without introducing any significant attenuation in the closed loop sensitivity from the target temperature source T_t to T_{ch}, as shown in Fig. 4. The proposed control law includes a reference model to diminish overshoots and an integral action to achieve zero steady state error in closed loop, even in the presence of constant ambient temperature disturbances. Experimental results showed that the standard deviation of T_{ch} was around 100μK as expected. Thus, the designed thermal isolation and regulation control system is well suited for the intended infrared imaging camera's purpose of accurately sensing the infrared source T_t.

6. ACKNOWLEDGMENTS

This project is supported by the DARPA IR program under grant N66001-00-C-8080.

7. REFERENCES

Anderson, Brian D. O. and John B. Moore (1989). *Optimal Control*. Prentice Hall.

Bitmead, Robert R., Michel Gevers and Vincent Wertz (1990). *Adaptive Optimal Control*. Prentice Hall.

Incropera, Frank P. and David P. DeWitt (1996). *Fundamentals of Heat and Mass Transfer*. 4rd ed.. John Wiley and Sons.

Ljung, Lennart (1999). *System Identification, Theory for the User*. 2nd ed.. Prentice Hall-Information and System sciences series.

Ott, Henry W. (1988). *Noise Reduction Techniques in Electronic Systems*. 2nd ed.. John Wiley and Sons.

Perazzo, T., M. Mao, O. Kwon, A. Majundar, J. B. Varesi and P. Norton (1999). Infrared vision using micro-optomechanical camera. *Applied Physics Letters* **74**, 3567–3569.

Sloman, A. W., Paul Buggs, James Molloy and Douglas Stewart (1996). A microcontroller-based driver to stabilize the temperature of an optical stage to within 1 mk in the range 4-38°c, using a peltier heat pump and a thermistor sensor. *Meas. Sci. Technol* **7**, 1653–1664.

Zhao, Y., J. Yamaguchi, J Choi, S. Morales, R. Horowitz, A. Majundar, P. Norton, J. Kitching, H. Lin, M.Athavale and J. Varesi (2001*a*). Design and fabrication of an optomechanical uncooled infrared imaging system. *Submitted to the International Mechanical Engineering Conference and Exposition*.

Zhao, Y., M. Mao, R. Horowitz, A. Majundar, J. Varesi, P. Norton and J. Kitching (2001*b*). Optomechanical uncooled infrared imaging system: Design, microfabrication and performance. *Submitted and accepted to JMEMS*.